Lattice finite-volume dependence of the nucleon parton distributions

Huey-Wen Lin and Rui Zhang

Phys. Rev. D **100**, 074502 — Published 4 October 2019

DOI: 10.1103/PhysRevD.100.074502

Lattice Finite-Volume Dependence of the Nucleon Parton Distributions

Huey-Wen Lin[1, 2, *] and Rui Zhang[1, †]

[1] *Department of Physics and Astronomy, Michigan State University, East Lansing, MI 48824*
[2] *Department of Computational Mathematics, Science & Engineering, Michigan State University, East Lansing, MI 48824*

There have been rapid developments in the direct calculation of the Bjorken-x dependence of parton distribution functions (PDFs) using lattice QCD, and the technique shows promising results. Among various new methods, large-momentum effective theory (LaMET), which calculates boosted hadron matrix elements of multiple spatial displacements on the lattice, shows promising PDFs at physical pion mass by both LP^3 and ETMC collaborations. However, the finite-volume systematics have not yet been studied, and it has been suggested that such systematics can be more significant for LaMET-type operators than the traditional bilinear quark operators in charges and form factors. In this work, we present the first study of the finite-volume systematic for both isovector nucleon unpolarized and helicity matrix elements on three lattice volumes (2.88, 3.84, 4.8 fm) with lattice spacing 0.12 fm and 220-MeV pion mass. We perform two-state simultaneous fits using multiple source-sink separations to remove excited-state contamination and obtain reliable ground-state matrix elements. We then implement nonperturbative renormalization and Fourier transform the matrix elements to momentum-space quasi-PDFs. Overall, we do not see significant finite-volume systematics at the studied boost momenta of $P_z = 1.3$ and 2.6 GeV.

I. INTRODUCTION

Recently, there have been rapid developments in lattice-QCD calculations of proton structure, especially in the parton distribution functions (PDFs). We overcame a longstanding obstacle and for the first time in lattice QCD are able to directly calculate the Bjorken-x dependence of the quark, helicity and transversity distributions. The PDFs are obtained using large-momentum effective theory (LaMET) [1], where the full Bjorken-x dependence of finite-momentum PDFs, called "quasi-PDFs", can be calculated on the lattice.[1] Following a nonperturbative renormalization of the parton quasi-distribution in a regularization-independent momentum-subtraction (RI/MOM) scheme [12, 13], we establish its matching to the $\overline{\text{MS}}$ PDFs and calculate the nonsinglet matching coefficient at next-to-leading order in perturbation theory [14, 15].[2] Parton distributions at physical pion mass have been calculated by multiple collaborations [21–26], showing very promising results in comparison with the global analysis of the parton distributions. However, these calculations are still, at the current stage, done on a single ensemble; in the best scenarios, some of the systematic uncertainties are estimated from more comprehensive studies of local operators [23, 24]. In this work, we perform the first study of the systematic uncertainties arising from finite-volume (FV) effects for the quasi-distributions.

Finite-volume effects are one of the main systematics in many lattice calculations, being significant for hadron masses and decay constants. It is essential to demonstrate either that the finite-volume effects are not relevant on the observable of interest at the volume used in the calculation, or that a reliable extrapolation to the infinite-volume limit is possible. The size of the finite-volume systematic depends on the quantities of interest; in general heavier hadrons have smaller systematics than lighter ones. Quantities such as the deuteron bound-state energy at the physical pion mass may require very large volumes, more than 20 fm. On the other hand, nucleon matrix elements such as the nucleon tensor charge g_T have been found to have small finite-volume effects by many independent studies [23, 27–30]. The operators used in LaMET calculations are usually bilocal operators connected by a spatial Wilson line, $\bar{\psi}(z_1)\Gamma U(z_1, z_2)\psi(z_2)$, and their dependence on lattice volume has not yet been studied, aside from the special case $z_1 = z_2$.

A recent work, Ref. [31], uses a toy model to demonstrate the effect of the spatial separation of two currents, attempting to address the finite-volume dependence in LaMET calculations. Within the framework of an effective scalar field theory, the authors work out a next-to-leading-order form for finite-volume effects on a spatially nonlocal

* hwlin@pa.msu.edu
† zhangr60@msu.edu

[1] In parallel, there have also been other proposals to calculate the PDFs in lattice QCD [2–11], which are subject to their own systematics. These approaches can be complementary to each other as well as to the LaMET approach.

[2] There has been some debate regarding whether the moments obtained from these nonlocal operators could be divergent [16, 17] without proper nonperturbative subtraction. Refs. [18, 19] explain that the only power divergence in the nonlocal-operator approach comes from the self-energy of the Wilson lines and can be properly treated such that it does to pose a problem for extraction of the PDFs. Ref. [20] used the Ioffe-time PDF approach [4], also involving nonlocal operators, and numerically demonstrated its consistency with the moment approach.

Ensemble ID	$L^3 \times L_t$	$M_\pi^{\rm val} L$	$t_{\rm sep}/a$	α	k	P_z	$N_{\rm cfg}$	$N_{\rm meas}$
a12m220S	$24^3 \times 64$	3.3	$\{6,7,8,9\}$	3.5	{2,3}	$\{3,6\}\frac{2\pi}{L}$	958	$\{22922, 45984, 45984, 61312\}$
a12m220M	$32^3 \times 64$	4.4	$\{6,7,8,9\}$	3	{2.5}	$\{4\}\frac{2\pi}{L}$	725	$\{11600, 23200, 23200, 46400\}$
a12m220L	$40^3 \times 64$	5.5	$\{6,7,8,9\}$	3.5	{3,4}	$\{5,10\}\frac{2\pi}{L}$	840	$\{13440, 26800, 26800, 53760\}$

TABLE I. Ensemble information and parameters used in this calculation. We use Gaussian momentum smearing [41] for the quark field $\psi(x) + \alpha \sum_j U_j(x) e^{ik\hat{e}_j} \psi(x+\hat{e}_j)$, where k is the input momentum-smearing parameter, $U_j(x)$ are the gauge links in the j direction, and α is a tunable parameter as in traditional Gaussian smearing.

current

$$\delta\text{FV} = \langle P|J(z,0)J(\mathbf{0},0)|P\rangle_{L-\infty} = A(z,L) \times \exp(-M(L-z)) + B(z,L) \times \exp(-m_\pi L) \tag{1}$$

where L is the spatial lattice size, z is the spatial separation of the nonlocal current J, M is the mass of the state studied, and the forms of $A(z,L)$ and $B(z,L)$, which could be polynomial in $L-z$, are interaction-dependent. This indicates that the finite-volume corrections of the nonlocal matrix element could be enhanced relative to their local counterparts, implying that a large lattice box is needed. Although this study may not directly apply to LaMET operators, a careful study of finite-volume systematics is needed to ensure that the LaMET PDF results do not suffer similar issues or worse.

In the case considered by Ref. [31], $z \approx L/4$ and a lattice size as large as $M_\pi L = 4$, the finite-volume discrepancy is roughly 10% of the final result. On the other hand, this effective theory has a region of validity $Mz \geq 1$. Reference [31] also claims a reconstruction of nonlocal lattice operators in a finite volume would be nontrivial and subject to Wilson-line renormalization. Whatever the case, an empirical study of FV effects across a range of lattice sizes should demonstrate whether they exhibit similar behavior to the above in the range of z of interest for nucleon structure.

In this work we study the finite-volume effects on the nucleon quasi-PDF matrix elements for both the unpolarized and helicity PDFs by calculating them on three different lattice spatial volumes. Our lattice setup and the detailed parameters can be found in Sec. II, the main numerical results and discussions in Sec. III, followed by conclusions in Sec. IV.

II. LATTICE PARAMETERS AND SETUP

This work is carried out with clover valence fermions on three ensembles with $a = 0.12$ fm, pion mass $M_\pi \approx 220$ MeV, and $N_f = 2+1+1$ (degenerate up/down, strange and charm) flavors of highly improved staggered dynamical quarks (HISQ) [32], generated by MILC Collaboration [33]. These three ensembles have three different spatial sizes $L \approx 2.88$, 3.84, 4.8 fm, which correspond to $M_\pi^{\rm val} L \approx 3.3$, 4.4 and 5.5, respectively. One-step hypercubic (HYP)-smeared gauge links [34] suppress discretization effects. The clover parameters are tuned to recover the lowest pion mass of the staggered quarks [29, 35–37]. The multigrid algorithm [38, 39] in Chroma software package [40] is used to speed up the clover fermion inversion of the quark propagators. We use Gaussian momentum smearing [41] for the quark field to improve our signal of the boosted-momentum proton state. Table I summarizes the momenta, source-sink separations, and statistics used in this work.

On the lattice, we calculate the following operators used in LaMET:

$$\mathcal{O}_\Gamma(z) = \bar{\psi}(z)\Gamma U(z,0)\psi(0), \tag{2}$$

where the spacelike Wilson line

$$U(z,0) = P\exp\left(-ig\int_0^z dz' A^z(z')\right). \tag{3}$$

$\Gamma = \gamma_t$ ($\gamma_z\gamma_5$) for unpolarized (longitudinally polarized, also called "helicity") PDFs[12, 42–44]. The hadron matrix element of $\mathcal{O}_\Gamma(z)$ can be directly obtained from lattice QCD, and its Fourier transformation is known as the quasi-PDF:

$$\tilde{q}(x, P_z, \tilde{\mu}) = \int_{-\infty}^{\infty} \frac{dz}{2\pi}\, e^{ixP_z z} \big\langle P\big|O_\Gamma(z)\big|P\big\rangle\,. \tag{4}$$

To make sure that we single out only the finite-volume effect rather the boost-momentum dependence of the quasi-PDFs, we calibrate two sets of momenta for this study. They are $P_z \approx 1.3$ and 2.6 GeV, which correspond to $\{3,4,5\}$

for "S", "M" and "L", and $\{6, 10\}$ for "S" and "L" ensembles, respectively, in units of lattice momentum with spatial periodic boundary conditions. At each nucleon boost momentum, $\widetilde{h}(z, P_z, a)$ is measured with multiple source-sink separations $t_{\rm sep}$ as listed in Table I. We investigate the excited-state contamination by performing "two-simRR" fits [37] using all $t_{\rm sep}$:

$$\begin{aligned} C_\Gamma^{\rm 3pt}(P_z, t, t_{\rm sep}) = & |\mathcal{A}_0|^2 \langle 0|\mathcal{O}_\Gamma|0\rangle e^{-E_0 t_{\rm sep}} \\ & + |\mathcal{A}_1||\mathcal{A}_0| \langle 1|\mathcal{O}_\Gamma|0\rangle e^{-E_1(t_{\rm sep}-t)} e^{-E_0 t} \\ & + |\mathcal{A}_0||\mathcal{A}_1| \langle 0|\mathcal{O}_\Gamma|1\rangle e^{-E_0(t_{\rm sep}-t)} e^{-E_1 t} \\ & + |\mathcal{A}_1|^2 \langle 1|\mathcal{O}_\Gamma|1\rangle e^{-E_1 t_{\rm sep}} + \ldots \end{aligned} \tag{5}$$

where E_0 (E_1) is the ground- (excited-) state nucleon energy and $\mathcal{A}_0$ ($\mathcal{A}_1$) are the overlapping and kinematic factors for the ground- (excited-) state nucleon, extracted from the two point correlators by fitting them to the form:

$$C^{\rm 2pt}(P_z, t) = |\mathcal{A}_0|^2 e^{-E_0 t} + |\mathcal{A}_1|^2 e^{-E_1 t} + \ldots \tag{6}$$

A few example fit plots from a subset of data on all three volumes with $P_z \approx 1.3$ and 2.6 GeV are shown in Figs. 1 and 2. One can clearly see that the simultaneous fits well describe data from all $t_{\rm sep}$, and the errors in the ground-state matrix-element extraction are not overconstrained by the smallest $t_{\rm sep}$ data. To check the consistency of the fits across source-sink separations, we show in Fig. 3 "two-simRR" fits to Eq. 5 using all, the largest 3, and the largest 2 source-sink separations from the a12m220L ensemble. As expected, the extracted ground-state matrix elements get noisier as we reduce the input data. We also compare the "two-sim" fit by dropping the last term in Eq. 5, the resulting matrix elements are consistent with the "two-simRR" fits using all $t_{\rm sep}$ and the statistical error size is similar. Therefore, we will use the ground-state matrix elements from "two-simRR" fits using all $t_{\rm sep}$.

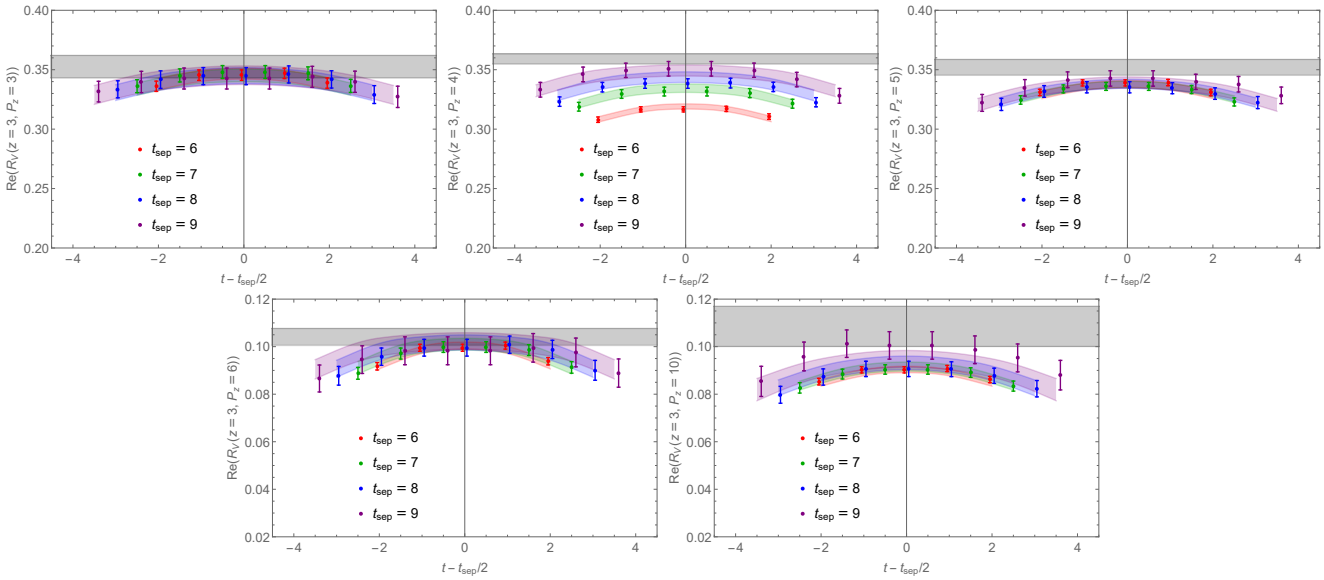

FIG. 1. Example three-point ratio plots $C_{\rm 3pt}(t)/C_{\rm 2pt}(t_{\rm sep})$ as functions of insertion time from the real unpolarized isovector nucleaon matrix elements with $z = 3$. The red, green, blue and purple bands are the reconstructed ratios from the fits to each source-sink separation $t_{\rm sep} = \{6, 7, 8, 9\}$, respectively, and the gray band shows the ground-state matrix elements from "two-simRR" fits in Eq. 5. The top two panels show the matrix elements from a12m220S, a12m220M and a12m220L (from left to right) for $P_z \approx 1.3$ GeV and the lower two plots show the the matrix elements from a12m220S and a12m220L for $P_z = 2.6$ GeV.

III. RESULTS AND DISCUSSION

Figures 4 and 5 summarize the final fitted bare isovector nucleon matrix elements for a range of positive z on all three ensembles for $P_z \approx 1.3$ and 2.6 GeV, respectively. These matrix elements are normalized by the real part of the $z = 0$ matrix elements for the unpolarized or polarized operator of each ensemble to improve the signal-to-noise

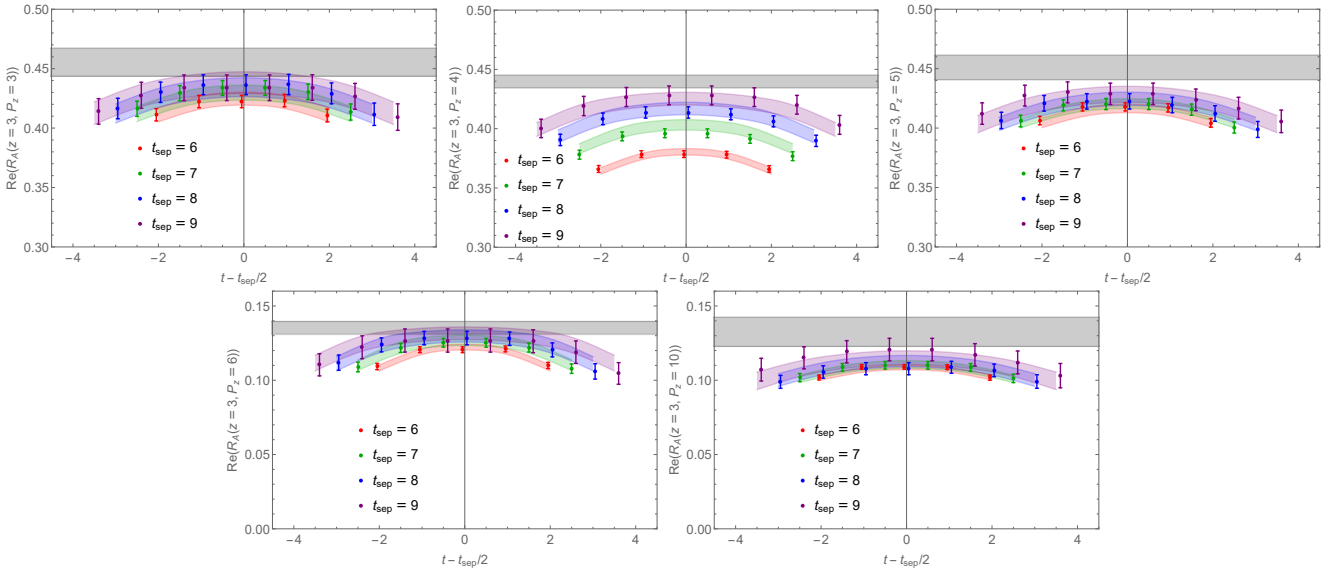

FIG. 2. Example three-point ratio plots $C_{3\mathrm{pt}}(t)/C_{2\mathrm{pt}}(t_{\mathrm{sep}})$ as functions of insertion time from the real polarized isovector nucleon nucleaon matrix elements with $z = 3$. The red, green, blue and purple bands are the reconstructed ratios from the fits to each source-sink separation $t_{\mathrm{sep}} = \{6, 7, 8, 9\}$, respectively, and the gray band shows the ground-state matrix elements from "two-simRR" fits in Eq. 5. The top two panels show the matrix elements from a12m220S, a12m220M and a12m220L (from left to right) for $P_z \approx 1.3$ GeV and the lower two plots show the the matrix elements from a12m220S and a12m220L for $P_z = 2.6$ GeV.

ratios of the data, as the same ratios are done in Refs. [15, 21–24]. We scale the matrix elements shown in Figs. 4 and 5 by a z-dependent function, $e^{0.15z}$, to boost the visibility of the smaller matrix elements at large z.) At small boost momentum $P_z \approx 1.3$ GeV, we found that for both unpolarized and polarized matrix elements, the central value of the real matrix elements are similar for all three volumes, while the central value of the imaginary matrix elements have more noticeable fluctuations as the volume increases. However, there is no clear trend of volume dependence. At large boost momentum $P_z \approx 2.6$ GeV, the bare matrix elements approach zero faster as the displacement z increases, which is expected; however, again, the small- and large-volume matrix elements are consistent within the statistical errors. Further, we noted that at this boost momentum (which is comparable to the boost momentum used in Refs. [15, 22–24]), the central values for the polarized matrix elements are closer between these two volumes than for the unpolarized ones.

We renormalize the nucleon matrix elements using a similar procedure as detailed in Refs. [15, 22, 23]. The nonperturbative renormalization (NPR) factor $Z(z, p_z^R, \mu_R, a)$ is calculated using the off-shell quark matrix element of $\hat{O}(z, a)$ in Landau gauge and requiring that all the loop corrections are canceled by $Z(z, p_z^R, \mu_R, a)$ at given p_z^R and μ_R, which are the Euclidean quark momentum in the z-direction and the off-shell quark momentum, respectively [12, 13]. The nonperturbative renormalization factor $Z(z, p_z^R, \mu_R, a)$ in the RI/MOM scheme is defined by imposing a condition on the quasi-PDF evaluated with off-shell quark states of momentum p with $p^2 \neq 0$, so that it matches the tree-level result at the given momentum.

$$\begin{aligned} & Z(z, p_z^R, \mu_R, a)^{-1} \langle S(z)\gamma^t U_z(z,0) S(0)\rangle\big|_{\substack{p^2=-\mu_R^2 \\ p_z=p_z^R}} \\ &= \langle S(z)\gamma^t W_z(z,0) S(0)\rangle\big|_{\mathrm{tree}} \\ &= e^{-izp_z} S(p)\gamma^t S(p)\big|_{p_z=p_z^R}\,, \end{aligned} \tag{7}$$

where the quark propagator $S(p)$ uses momentum source, and NPR vertices $S(z)\gamma^t U_z(z,0)S(0)$ are computed on all three lattice ensembles individually. The NPR factors are then obtained from

$$Z(z, p_z^R, \mu_R, a) = \frac{e^{izp_z}}{12} \mathrm{Tr}\left[\langle S(p)\rangle^{-1} \langle S(z)\gamma^t W_z(z,0) S(0)\rangle \langle S(p)\rangle \gamma^t\right]\Big|_{\substack{p^2=-\mu_R^2 \\ p_z=p_z^R}}. \tag{8}$$

For convenience, we choose $\widetilde{h}_R(z, P_z, p_z^R, \mu_R)$ at $\mu_R = 2.4$ GeV and $p_z^R = 0$ GeV for this quasi-distribution comparison. Fig. 6 shows the scaled renormalization factors for the unpolarized and polarized nucleon matrix elements for all three

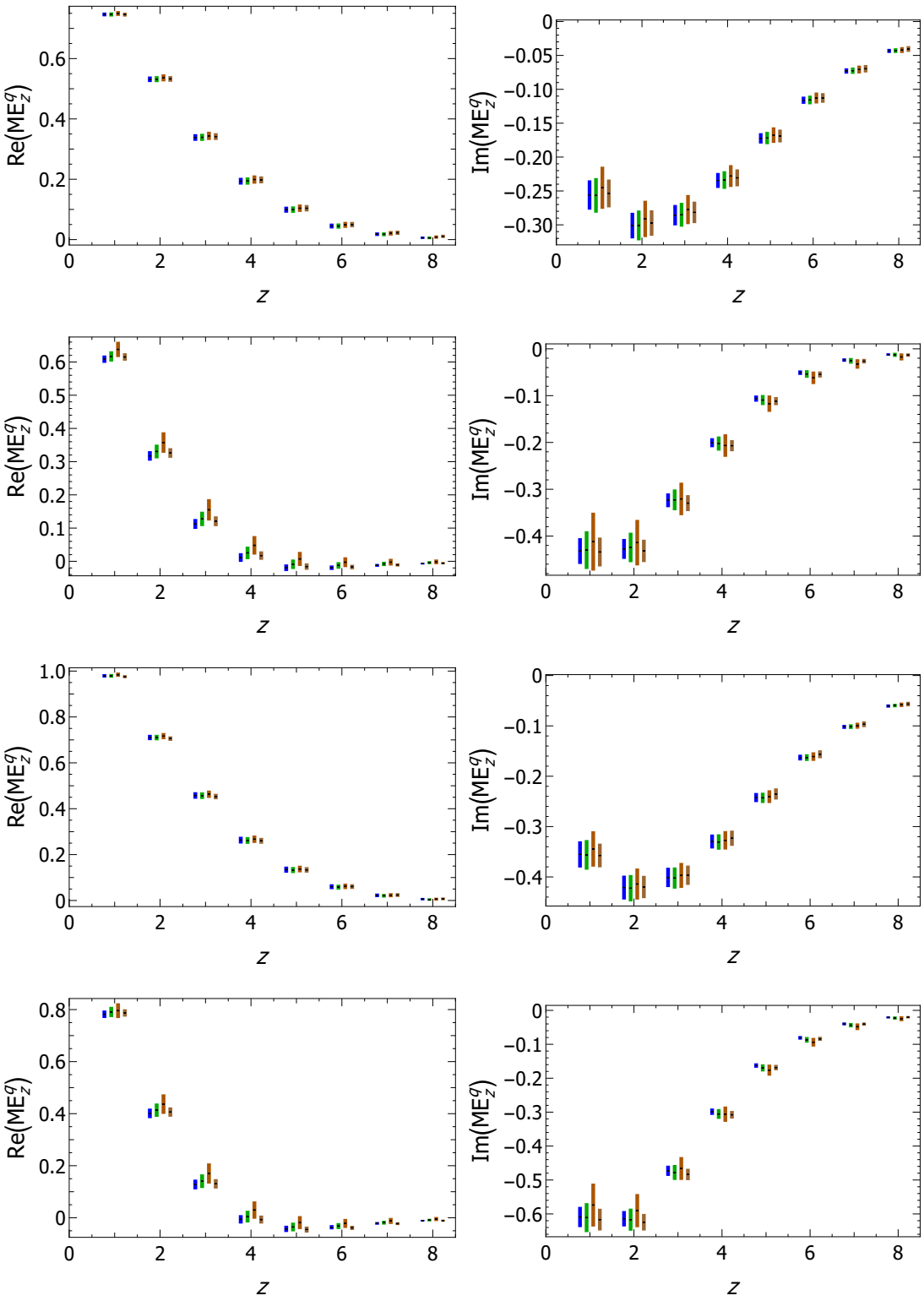

FIG. 3. Example multistate-fitting real (left column) and imaginary (right column) matrix-element comparison from the a12m220L ensemble with $P_z = 1.3$ (first and third rows) and 2.6 GeV (second and fourth rows) data as a function of Wilson-line displacement for unpolarized (top-2 rows) and polarized (bottom-2 rows) matrix elements. The data points from left to right indicates "two-simRR" fits (i.e. using all three terms in Eq. 5) using source-sink seperation $t_{\rm sep} \in [6, 9]$, $[7, 9]$, $[8, 9]$ respectively and "two-sim" fit (i.e. by not using the last term in Eq. 5) to $t_{\rm sep} \in [8, 9]$, showing consistent fits across different input of source-sink separation data.

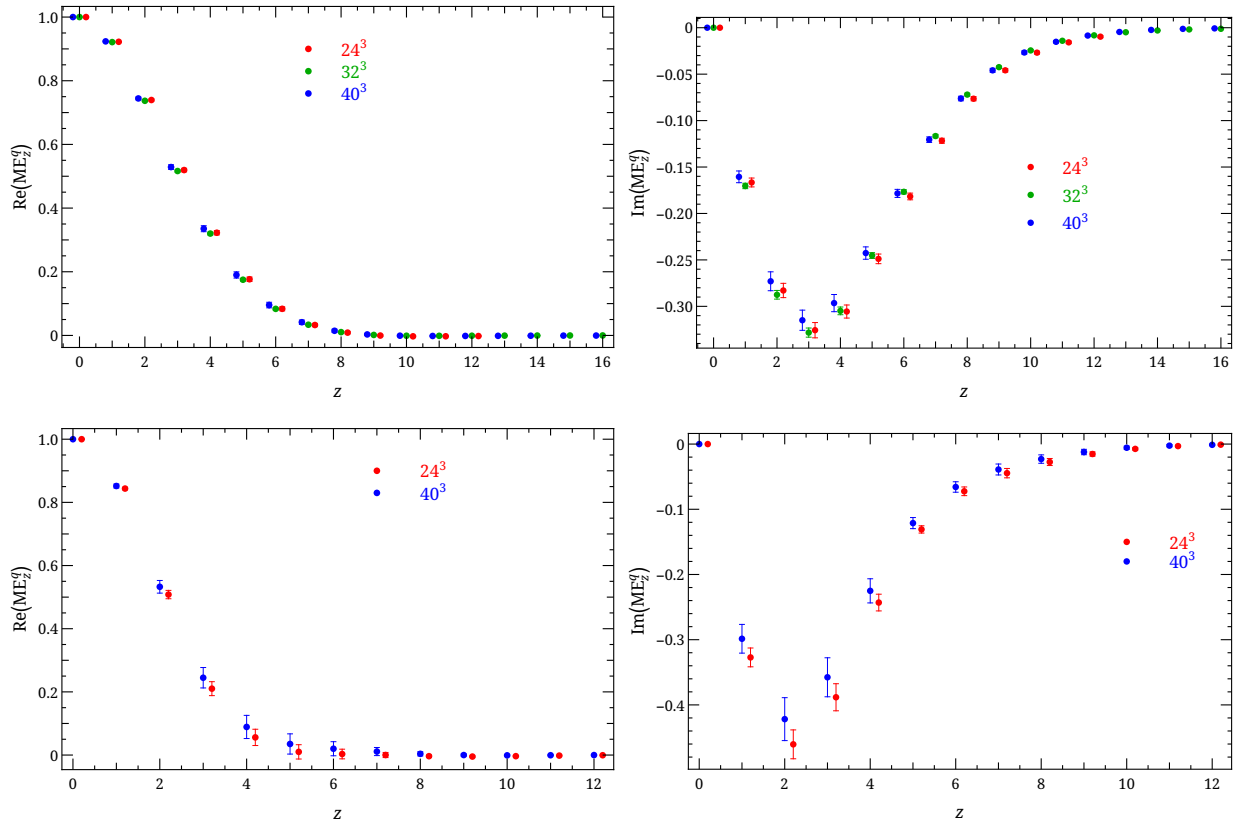

FIG. 4. The normalized $P_z \approx 1.3$ GeV (top) and $P_z \approx 2.6$ GeV (bottom) bare isovector nucleon matrix elements for unpolarized PDFs as functions of z at the three volumes ($M_\pi L = 3.3$, 4.4 and 5.5 indicated by red, green and blue, respectively).

volumes. The volume-dependence of the renormalization factors is milder than that of the matrix elements themselves. The renormalized matrix element $\widetilde{h}_R(z, P_z, p_z^R, \mu_R) = \widetilde{Z}^{-1}(z, p_z^R, \mu_R, a)\widetilde{h}(z, P_z, a)$ inherits the dependence on p_z^R and μ_R, which is supposed to be canceled after the later matching step to recover for lightcone distribution. However, in this work, we are only interested in the finite-volume effects and thus will skip the one-loop matching.

Next, we need to Fourier transform the $\widetilde{h}_R(z, P_z, p_z^R, \mu_R)$ into x-space to obtain the quasi-distribution $\delta\widetilde{q}(x, P_z, p_z^R, \mu_R)$. As originally pointed out in Ref. [21] in 2017 and demonstrated using CT14 NNLO [45] at 2 GeV, a naive Fourier transform from momentum-space x to coordinate space z and then back suffers an inverse problem. This means that since the lattice calculation has finite displacement z in the nonlocal operator and cannot actually use infinitely boosted momentum, a straightforward Fourier transform produces truncation effects, resulting in unphysical oscillatory behavior, as observed in earlier works [12, 46]. The antiquark and small-x regions suffer the maximum deformation. In Ref. [21], two ideas ("filter" and "derivative" methods) were proposed to remove this biggest systematic uncertainty in the LaMET approach to studying x-dependent hadron structure: Fourier-transformation truncation. When not assuming a parametrization form, this determines the shape of the PDF. The first lattice PDF at physical pion mass was used to demonstrate how the proposed methods improve real-world lattice calculations. A third method was proposed in late 2017, modifying the Fourier transformation in LaMET using a single-parameter Gaussian weight [47]. As this manuscript was completed, another three methods were proposed in Ref. [48]. Following the recent work in Refs. [22–24], we adopt the simple but effective "derivative" method:

$$\tilde{Q}(x, P_z, p_z^R, \mu_R) = i \int_{-z_{\max}}^{+z_{\max}} dz\ e^{ixP_z z} \tilde{h}'_R(z, P_z, p_z^R, \mu_R)/x, \tag{9}$$

where $\tilde{Q}$ is quasi-PDF ($q(x)$, $\Delta q(x)$ and $\delta q(x)$ respectively), and $\tilde{h}'_R$ is the derivative of the renormalized matrix elements for the corresponding operator.

For the purpose of this finite-volume study, we pick $z_{\max} = 12$ in the Fourier transformation. The isovector nucleon quasi-PDF distribution results are shown in Fig. 7. The errors shown here are statistical only. In the $P_z \approx 2.6$ GeV case, we see a more noticeable difference in volume dependence, most likely due to statistical fluctuation. The

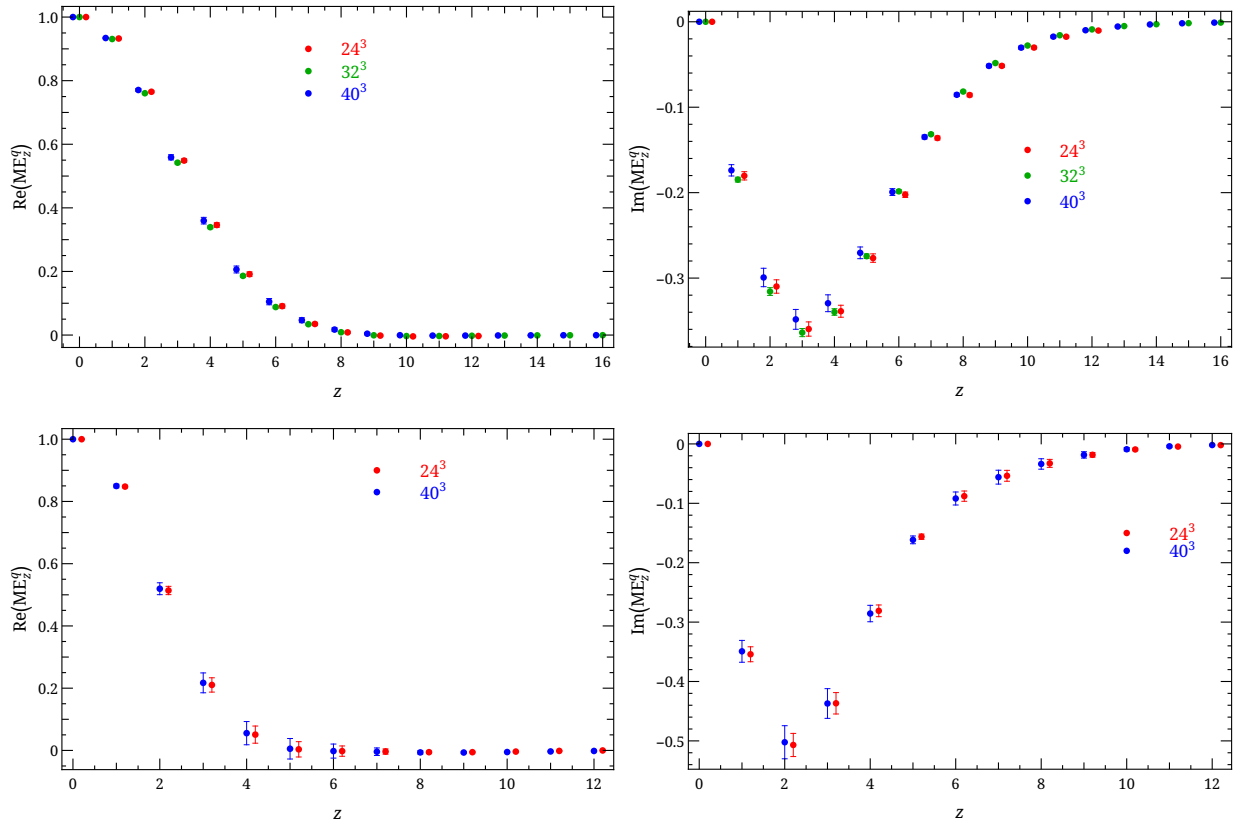

FIG. 5. The normalized $P_z \approx 1.3$ GeV (top) and $P_z \approx 2.6$ GeV (bottom) bare isovector nucleon matrix elements for polarized PDFs as functions of z at the three volumes ($M_\pi L = 3.3$, 4.4 and 5.5 indicated by red, green and blue, respectively). Given the apparently quite small size of the finite-volume effects, it is certainly difficult to discern them on the figure.

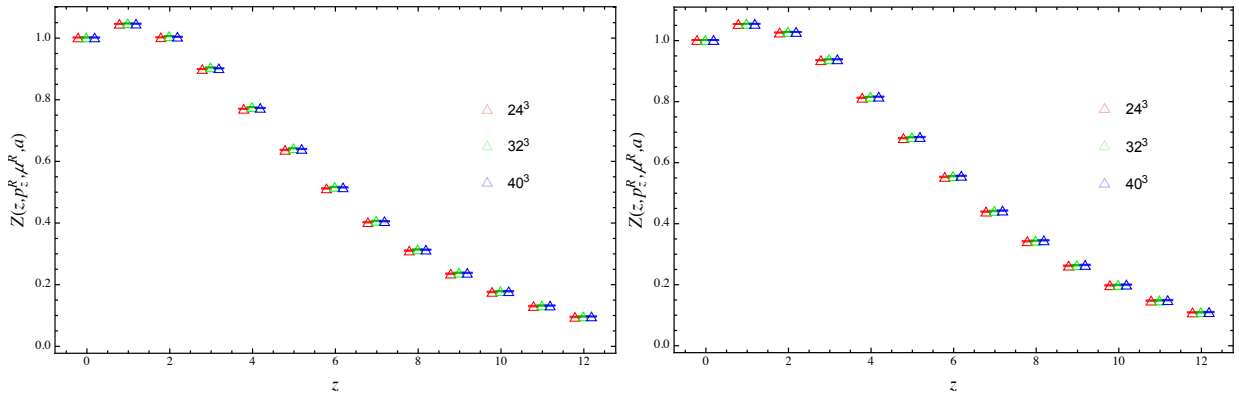

FIG. 6. The normalized unpolarized (left) and polarized (right) NPR factors as a function of the Wilson line length for lattice spaial size 24 (red), 32 (green) and 40 (blue). For $p_z^R = 0$, the imaginary parts vanish so are not shown. The renormalization constants are scaled by an exponential factor $\exp(0.1z)$ so that the large-z points can be seen more clearly.

distribution for both volumes are aligned well for most of the positive-x region, while in the negative-x region there is a more noticeable difference in the central values of the quasi-distribution. Nonetheless, they are consistent within the statistical errors. These differences in central values become less important when systematics from scale dependence of NPR renormalization, $z_{\max}$ dependence in Fourier transformation and one-loop matching, are included, as done in Refs. [22–24].

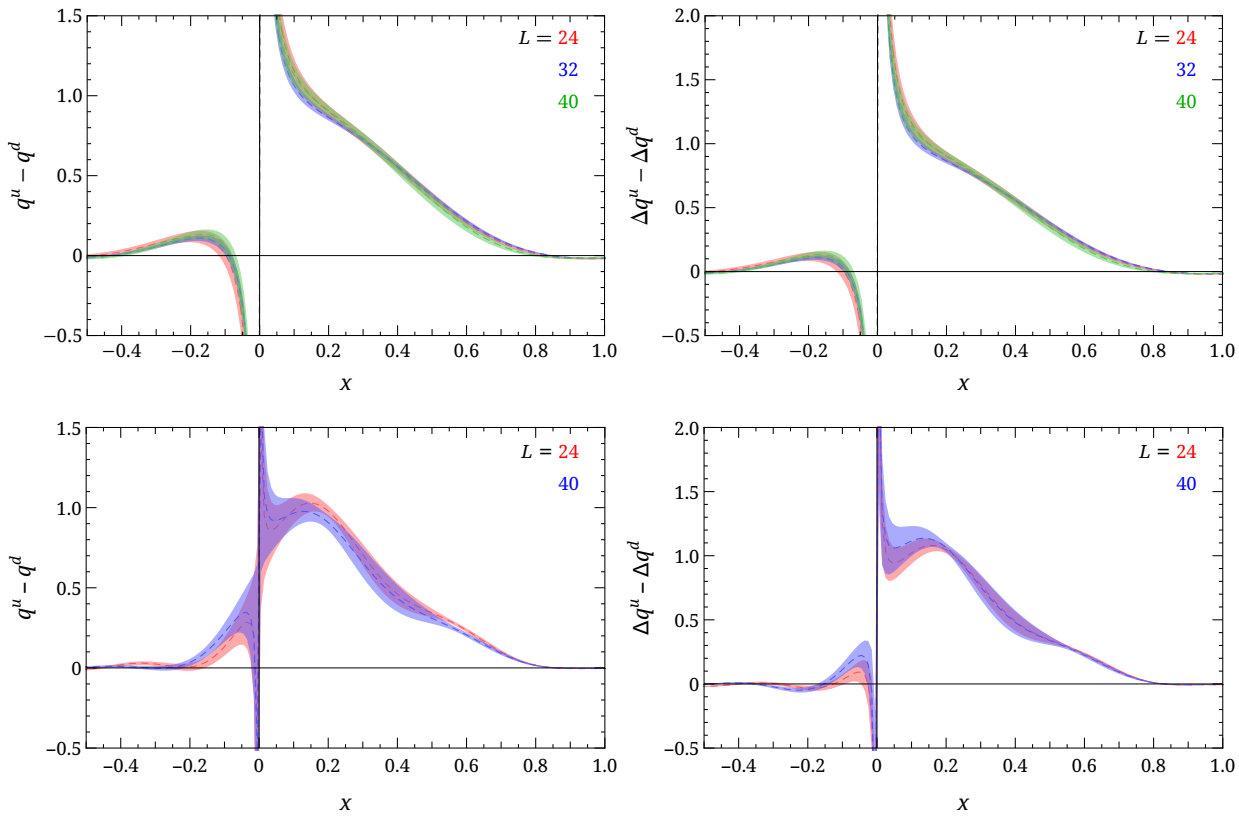

FIG. 7. The quasi-distribution of nucleon isovector unpolarized (left) and polarized PDFs (right) with data from $P_z \approx 1.3$ (top) and 2.6 (bottom) GeV. Only the statistical errors are shown in the figures. The finite-volume effects are small for both distributions.

IV. SUMMARY

To summarize, we have calculated the isovector nucleon matrix elements with spatially displaced nonlocal operators using three lattice volumes (2.88, 3.84, 4.8 fm) at a fixed single pion mass of 220 MeV and lattice spacing 0.12 fm. This is the first finite-volume study of these new operators used in lattice-QCD calculations. After carefully extracting the bare matrix elements for unpolarized and polarized distribution, we do not observe noticeable volume dependence in these ensembles. We further checked the quasi-PDF distribution after applying NPR, and the quasi-distribution remain consistent within statistical errors. We conclude that finite-volume dependence does not play a significant role for the boosted nucleon matrix elements used for quasi-distributions within the range of $M_\pi^{\rm val} L \in \{3.3, 5.5\}$.

ACKNOWLEDGMENTS

We thank the MILC Collaboration for sharing the lattices used to perform this study. The LQCD calculations were performed using the Chroma software suite [40]. This research used resources of the National Energy Research Scientific Computing Center, a DOE Office of Science User Facility supported by the Office of Science of the U.S. Department of Energy under Contract No. DE-AC02-05CH11231 through ERCAP; facilities of the USQCD Collaboration, which are funded by the Office of Science of the U.S. Department of Energy, and supported in part by Michigan State University through computational resources provided by the Institute for Cyber-Enabled Research. HL and RZ are supported by the US National Science Foundation under grant PHY 1653405 "CAREER: Constraining Parton

Distribution Functions for New-Physics Searches".

[1] X. Ji, J.-H. Zhang, and Y. Zhao, Phys. Rev. Lett. **111**, 112002 (2013), arXiv:1304.6708 [hep-ph].
[2] Y.-Q. Ma and J.-W. Qiu, Phys. Rev. **D98**, 074021 (2018), arXiv:1404.6860 [hep-ph].
[3] Y.-Q. Ma and J.-W. Qiu, Phys. Rev. Lett. **120**, 022003 (2018), arXiv:1709.03018 [hep-ph].
[4] A. V. Radyushkin, Phys. Rev. **D96**, 034025 (2017), arXiv:1705.01488 [hep-ph].
[5] K. Orginos, A. Radyushkin, J. Karpie, and S. Zafeiropoulos, Phys. Rev. **D96**, 094503 (2017), arXiv:1706.05373 [hep-ph].
[6] K.-F. Liu and S.-J. Dong, Phys. Rev. Lett. **72**, 1790 (1994), arXiv:hep-ph/9306299 [hep-ph].
[7] J. Liang, K.-F. Liu, and Y.-B. Yang, *Proceedings, 35th International Symposium on Lattice Field Theory (Lattice 2017): Granada, Spain, June 18-24, 2017*, EPJ Web Conf. **175**, 14014 (2018), arXiv:1710.11145 [hep-lat].
[8] W. Detmold and C. J. D. Lin, Phys. Rev. **D73**, 014501 (2006), arXiv:hep-lat/0507007 [hep-lat].
[9] V. Braun and D. Müller, Eur. Phys. J. **C55**, 349 (2008), arXiv:0709.1348 [hep-ph].
[10] G. S. Bali *et al.*, *Proceedings, 35th International Symposium on Lattice Field Theory (Lattice 2017): Granada, Spain, June 18-24, 2017*, Eur. Phys. J. **C78**, 217 (2018), arXiv:1709.04325 [hep-lat].
[11] A. J. Chambers, R. Horsley, Y. Nakamura, H. Perlt, P. E. L. Rakow, G. Schierholz, A. Schiller, K. Somfleth, R. D. Young, and J. M. Zanotti, Phys. Rev. Lett. **118**, 242001 (2017), arXiv:1703.01153 [hep-lat].
[12] J.-W. Chen, T. Ishikawa, L. Jin, H.-W. Lin, Y.-B. Yang, J.-H. Zhang, and Y. Zhao, Phys. Rev. **D97**, 014505 (2018), arXiv:1706.01295 [hep-lat].
[13] C. Alexandrou, K. Cichy, M. Constantinou, K. Hadjiyiannakou, K. Jansen, H. Panagopoulos, and F. Steffens, Nucl. Phys. **B923**, 394 (2017), arXiv:1706.00265 [hep-lat].
[14] I. W. Stewart and Y. Zhao, Phys. Rev. **D97**, 054512 (2018), arXiv:1709.04933 [hep-ph].
[15] Y.-S. Liu, J.-W. Chen, L. Jin, H.-W. Lin, Y.-B. Yang, J.-H. Zhang, and Y. Zhao, (2018), arXiv:1807.06566 [hep-lat].
[16] G. C. Rossi and M. Testa, Phys. Rev. **D96**, 014507 (2017), arXiv:1706.04428 [hep-lat].
[17] G. Rossi and M. Testa, Phys. Rev. **D98**, 054028 (2018), arXiv:1806.00808 [hep-lat].
[18] X. Ji, J.-H. Zhang, and Y. Zhao, Nucl. Phys. **B924**, 366 (2017), arXiv:1706.07416 [hep-ph].
[19] A. V. Radyushkin, Phys. Lett. **B788**, 380 (2019), arXiv:1807.07509 [hep-ph].
[20] J. Karpie, K. Orginos, and S. Zafeiropoulos, JHEP **11**, 178 (2018), arXiv:1807.10933 [hep-lat].
[21] H.-W. Lin, J.-W. Chen, T. Ishikawa, and J.-H. Zhang (LP3), Phys. Rev. **D98**, 054504 (2018), arXiv:1708.05301 [hep-lat].
[22] J.-W. Chen, L. Jin, H.-W. Lin, Y.-S. Liu, Y.-B. Yang, J.-H. Zhang, and Y. Zhao, (2018), arXiv:1803.04393 [hep-lat].
[23] H.-W. Lin, J.-W. Chen, X. Ji, L. Jin, R. Li, Y.-S. Liu, Y.-B. Yang, J.-H. Zhang, and Y. Zhao, Phys. Rev. Lett. **121**, 242003 (2018), arXiv:1807.07431 [hep-lat].
[24] Y.-S. Liu, J.-W. Chen, L. Jin, R. Li, H.-W. Lin, Y.-B. Yang, J.-H. Zhang, and Y. Zhao, (2018), arXiv:1810.05043 [hep-lat].
[25] C. Alexandrou, K. Cichy, M. Constantinou, K. Jansen, A. Scapellato, and F. Steffens, Phys. Rev. Lett. **121**, 112001 (2018), arXiv:1803.02685 [hep-lat].
[26] C. Alexandrou, K. Cichy, M. Constantinou, K. Jansen, A. Scapellato, and F. Steffens, Phys. Rev. **D98**, 091503 (2018), arXiv:1807.00232 [hep-lat].
[27] R. Gupta, Y.-C. Jang, B. Yoon, H.-W. Lin, V. Cirigliano, and T. Bhattacharya, Phys. Rev. **D98**, 034503 (2018), arXiv:1806.09006 [hep-lat].
[28] T. Bhattacharya, V. Cirigliano, S. Cohen, R. Gupta, H.-W. Lin, and B. Yoon, Phys. Rev. **D94**, 054508 (2016), arXiv:1606.07049 [hep-lat].
[29] T. Bhattacharya, V. Cirigliano, S. Cohen, R. Gupta, A. Joseph, H.-W. Lin, and B. Yoon (PNDME), Phys. Rev. **D92**, 094511 (2015), arXiv:1506.06411 [hep-lat].
[30] J. R. Green, J. W. Negele, A. V. Pochinsky, S. N. Syritsyn, M. Engelhardt, and S. Krieg, Phys. Rev. **D86**, 114509 (2012), arXiv:1206.4527 [hep-lat].
[31] R. A. Briceño, J. V. Guerrero, M. T. Hansen, and C. J. Monahan, Phys. Rev. **D98**, 014511 (2018), arXiv:1805.01034 [hep-lat].
[32] E. Follana, Q. Mason, C. Davies, K. Hornbostel, G. P. Lepage, J. Shigemitsu, H. Trottier, and K. Wong (HPQCD, UKQCD), Phys. Rev. **D75**, 054502 (2007), arXiv:hep-lat/0610092 [hep-lat].
[33] A. Bazavov *et al.* (MILC), Phys. Rev. **D87**, 054505 (2013), arXiv:1212.4768 [hep-lat].
[34] A. Hasenfratz and F. Knechtli, Phys. Rev. **D64**, 034504 (2001), arXiv:hep-lat/0103029 [hep-lat].
[35] R. Gupta, Y.-C. Jang, H.-W. Lin, B. Yoon, and T. Bhattacharya, Phys. Rev. **D96**, 114503 (2017), arXiv:1705.06834 [hep-lat].
[36] T. Bhattacharya, V. Cirigliano, R. Gupta, H.-W. Lin, and B. Yoon, Phys. Rev. Lett. **115**, 212002 (2015), arXiv:1506.04196 [hep-lat].
[37] T. Bhattacharya, S. D. Cohen, R. Gupta, A. Joseph, H.-W. Lin, and B. Yoon, Phys. Rev. **D89**, 094502 (2014), arXiv:1306.5435 [hep-lat].
[38] R. Babich, J. Brannick, R. C. Brower, M. A. Clark, T. A. Manteuffel, S. F. McCormick, J. C. Osborn, and C. Rebbi, Phys. Rev. Lett. **105**, 201602 (2010), arXiv:1005.3043 [hep-lat].
[39] J. C. Osborn, R. Babich, J. Brannick, R. C. Brower, M. A. Clark, S. D. Cohen, and C. Rebbi, *Proceedings, 28th International Symposium on Lattice field theory (Lattice 2010): Villasimius, Italy, June 14-19, 2010*, PoS **LATTICE2010**,

037 (2010), arXiv:1011.2775 [hep-lat].
[40] R. G. Edwards and B. Joo (SciDAC, LHPC, UKQCD), *Lattice field theory. Proceedings, 22nd International Symposium, Lattice 2004, Batavia, USA, June 21-26, 2004*, Nucl. Phys. Proc. Suppl. **140**, 832 (2005), [,832(2004)], arXiv:hep-lat/0409003 [hep-lat].
[41] G. S. Bali, B. Lang, B. U. Musch, and A. Schäfer, Phys. Rev. **D93**, 094515 (2016), arXiv:1602.05525 [hep-lat].
[42] Y. Hatta, X. Ji, and Y. Zhao, Phys. Rev. **D89**, 085030 (2014), arXiv:1310.4263 [hep-ph].
[43] J.-W. Chen, T. Ishikawa, L. Jin, H.-W. Lin, J.-H. Zhang, and Y. Zhao, (2017), arXiv:1710.01089 [hep-lat].
[44] M. Constantinou and H. Panagopoulos, Phys. Rev. **D96**, 054506 (2017), arXiv:1705.11193 [hep-lat].
[45] S. Dulat, T.-J. Hou, J. Gao, M. Guzzi, J. Huston, P. Nadolsky, J. Pumplin, C. Schmidt, D. Stump, and C. P. Yuan, Phys. Rev. **D93**, 033006 (2016), arXiv:1506.07443 [hep-ph].
[46] J. Green, K. Jansen, and F. Steffens, Phys. Rev. Lett. **121**, 022004 (2018), arXiv:1707.07152 [hep-lat].
[47] T. Ishikawa, L. Jin, H.-W. Lin, A. Schäfer, Y.-B. Yang, J.-H. Zhang, and Y. Zhao, Sci. China Phys. Mech. Astron. **62**, 991021 (2019), arXiv:1711.07858 [hep-ph].
[48] J. Karpie, K. Orginos, A. Rothkopf, and S. Zafeiropoulos, JHEP **04**, 057 (2019), arXiv:1901.05408 [hep-lat].